FINAL DEGREE THESIS IN BIOMEDICAL ENGINEERING DEGREE

ANALYSIS OF THE BIOMECHANICAL BEHAVIOUR OF HEALTHY, DEGENERATED AND PMMA CEMENTED PIG LUMBAR INTERVERTEBRAL DISCS

AUTHOR: GUILLERMO COLLADO SORIA

SUPERVISOR: LUCA CRISTOFOLINI

Academic year: 2018-19

Abstract

Lower Back Pain (LBP) is a common issue that affects especially to the elderly. One of its principal causes is the intervertebral disc degeneration, having a strong influence in motion and human body posture. Due to this, there is a special interest in studying the behaviour of the spine in dynamic and static conditions by non-invasive methods to understand the degeneration consequences and possible solutions as the Percutaneous Cemented Discoplasty (PCD). In this study, it is highlighted the Digital Image Correlation (DIC), which consists of a non-invasive acquisition of the biomechanical distribution of displacements and deformations in a full-field model with accuracy and precision.

In order to study the impact of the intervertebral disc degeneration, the specimens under investigation were healthy, unhealthy and PMMA cemented pig lumbar spine segments that were submitted to flexion, extension and lateral bending in order to replicate the normal human motion. Using the 3D-DIC method it was possible to compare the biomechanical behaviours of each pig specimen in an effective way, demonstrating an intervertebral disc height increase through PCD technique that could reduce significantly LBP derived from the loss of height in degeneration.

Acknowledgments

INDEX

1. INTRODUCTION

1.1. Lumbar spine degeneration: consequences and interest

The spine is a very important part of the musculoskeletal system whose function is to support the upper body weight, to protect the organs and the spinal cord and to ensure body mobility [1]. Due to that, it is interesting to know what causes spine diseases and their consequences.

Particularly, the lumbar spine is the level that sustains more weight because it supports the upper body. This produces a long-term spine deterioration that entails to the lower back pain (LBP), one of the most common health problems that limits the activity of the people, especially in the elderly. Moreover, some investigations as Hoy et al. and Adams et al. defend that this kind of disease is likely going to increase over the next years [2], [3].

A correlation between intervertebral disc degeneration and the spine pain has been documented [4], but LBP can be also caused by multiple factors, especially the aging [3], [5], body posture [6] and repetitive loads that lead to fatigue [3], [5]. It has been discovered genetical influences in intervertebral disc degeneration, explaining 70% of the variance in lumbar and cervical spines [7].

A degenerated intervertebral disc can have any of its anatomical parts (nucleus pulposus, annulus fibrosus and cartilaginous endplates) injured (Figure 1), leading to a loss of height [8], strength or a sclerosis respectively [9] and also showing a disturbed stress distribution [8], [9]. The nucleus pulposus is a mucoid protein that regulates the pressure and height of the disc because of its capacity of water absorption [5]. However, it shows the biggest impact in intervertebral disc degeneration [8] reducing its water absorption capacity and consequently its height [12]. This water loss transfers the stress concentration from the nucleus pulposus to the annulus [11] that in flexion it leads to a massive load in vertebrae [13].

In this study, it is hypothesized that the loss of intervertebral disc height entails to an intervertebral foramen size reduction that squeezes the spinal nerve (Figure 1). Spinal nerves originate from the spinal cord in the posterior part of the spine, and it can be damaged if the space between adjacent vertebrae (intervertebral foramen) is reduced, producing LBP.
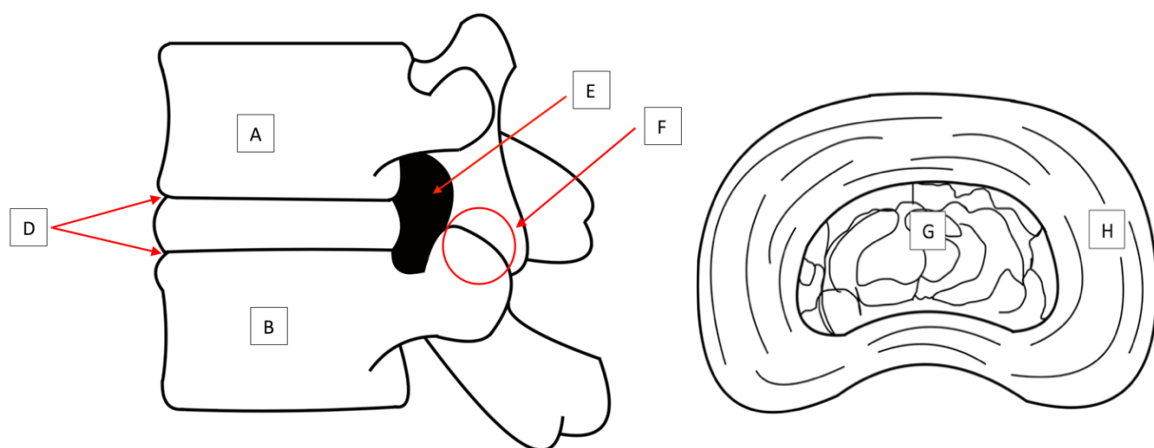

Figure 1. Representation of a 2-level vertebra segment in the lateral view (left) and an intervertebral disc in the axial view (right). A: Upper vertebra; B: Lower vertebra; C: Intervertebral disc; D: Endplates; E: Vertebral foramen; F: Facet joint; G: Nucleus pulposus; H: Annulus fibrosus.

Due to this, there is a special interest in studying the spine behaviour in dynamic and static conditions to understand the mechanisms responsible of the disease and to provide an adapted treatment for the patient suffering from LBP. In vivo studies have been performed to assess the stability of the spine with an intradiscal transducer across the intervertebral disc [11], [13], [14], [15], [16], [17], in order to measure the strains and displacements allowing the characterization of biological tissues and their interactions with biological devices [18].

However, it has to be considered that investigations in a living body are preferred to be minimally-invasive and secure to subject tests, what limits the range of possible procedures and the subjects of the study. An alternative to this limitation is to investigate on surrogates, in particular in vitro cadaveric specimens, to develop reliable clinical methods for patients.

Therefore, it is necessary to make preliminary tests in cadaveric specimens. In this project, spines were removed from porcine cadavers in order to find modern alternatives that can reproduce an injured patient condition in the most similar way possible. Animal specimens are compatible alternatives to human models due to their efficiency [9] [19].

1.2. Degeneration solution: history, discoplasty and alternatives

Even though total disc replacement is still an incomplete field of study that needs more experimentation [20], it has been an accepted solution for spine degeneration developed since a few years ago [21]. However, it is a highly-invasive method that requires open surgery which lasts hours, dedication and precision from the clinicians and also needs to be taken with attention because of the risks of such a surgery.

Another promising alternative is tissue engineering, consisting of a cell-based therapy cultivated and injected in the spine to replace the injured intervertebral disc [22]. These tissue-engineered therapies are being developed to reduce the intervertebral disc injury by stabilizing the disorder of stress distribution [23].

Nowadays, the use of biomaterials shows an effective reparation or substitution of a degenerated intervertebral disc. Some of the applications are hydrogels as a nucleus pulposus role and sealants for the annulus fibrosus fissures [8]. In this study, it is studied the percutaneous cement discoplasty (PCD), based on a surgery that consists of injecting cement in the intervertebral disc in order to improve the stabilization of an unhealthy spine. Some authors such as Varga et al. and Sola et al. had used this non-invasive surgical method injecting polymethyl methacrylate (PMMA) from the posterior part of the spine, having as results a gain of stability, spine deviation reduction and less pain and disability [24], [25]. The use of PMMA successfully fills the intervertebral disc and distributes the load in the endplates.

On this study, it was implemented the PCD treatment in vitro to investigate its features and properties to verify if the PMMA injection increase significantly the intervertebral disc height and consequently improves the spine disease without compromising the spine motion.

1.3. Digital Image Correlation

In order to avoid any invasive method as the previously cited intradiscal transducer, the biomechanical behaviour has been studied using a Finite Element Method (FEM) defining the geometry and material properties from a previously scanned spine by Computed Tomography (CT) [26] or modelled and simulated by computer [27], [28], [29].

Nowadays, the Digital Image Correlation (DIC) is a relatively new method that is becoming important in this field of study. It consists of a non-invasive measurement method that records the full-field of displacements and strains [30]. This technique has his appearance in the early 70', increasing its popularity especially in micro and nanomechanical testing [31]. This technique started to be applied to biomechanics in the late 90' [32], giving the subject-specific response from a selected part of the body imposed to a load and registering the biomechanical distribution of deformations of the sample surface with accuracy and precision [33]. The correlation is done using multiple images giving a 3D representation of the sample [18].

There are other related techniques as the Digital Volume Correlation (DVC) that allows measuring strain distribution inside the vertebra. However, it is affected by the time-consuming procedure of images acquisition, being required to scan the specimen previously with micro-CT to evaluate the reliability of DVC. This could be a problem with viscoelastic specimens [34]. Nevertheless, the improvement of the micro-CT has given attention to the DVC examination of trabecular and cortical bones and bone-cement interfaces [18].

The applications that the DIC method provide are innumerable due to its versatility in different dimensional scales and biological specimens [18]. In this project, the DIC system was used to compare the strain distribution differences between a healthy lumbar spine, an unhealthy lumbar spine and also a PCD treated unhealthy lumbar spine.

1.4. Objectives

Starting from a healthy lumbar spine segment previously removed from a porcine cadaver, cleaned and prepared for testing (read 2.1.), it was applied a load under the DIC recording in flexion, extension and lateral bending (read 2.4.2.). Consecutively, the nucleus pulposus was removed to reproduce the unhealthy segment and it was submitted to the same conditions (read 2.4.3.). Finally, the empty nucleus pulposus was filled with the PMMA cementation based on the PCD and also tested in the same conditions (read 2.4.4.) (Figure 2).
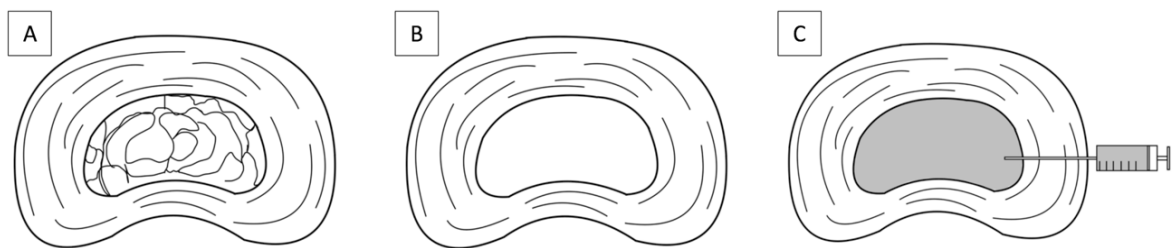

Figure 2. Conditions of the specimen. A: Healthy/intact; B: Unhealthy/degenerated; C: Cemented/discoplasty.

The objective of this study was to compare the DIC computed motion for each specimen in different health conditions and discuss if the PCD was able to recover the anatomical and physiological properties lost in a degenerated lumbar spine.

As for every software used in subject-specific modelling, before applying the DIC method it was required to optimize the system and specimen surface parameters to ensure the best testing condition and minimizing the recorded total error that would depend on the sample of interest and the environmental surroundings [18], [30] (read 2.3.). Likewise, the total error was composed by the systematic error (a mean error originated by the instrument) and the random error (irregular error impossible to control). Getting the optimal parameters for the study, it was possible to detect the possible failures from a specific porcine spine motion in order to improve or investigate new surgical techniques to solve this kind of problems [35].

2. MATERIALS AND METHODS

2.1. Preparation of the specimen

The pig spine has been obtained from a slaughterhouse in accordance with ethical regulation from a young individual animal. The specimens under investigation were 11 pig lumbar spine segments composed of the intervertebral disc between 2 vertebrae: 3 T13-L1 level, 1 T15-L1 level, 6 L3-L4 level and 1 L5-L6 level segments *.

The cleaning procedure consisted of preserving the elements of interest (intervertebral disc, vertebra and facet joints), removing surrounding soft tissues and ligaments except the anterior and supraspinous ligaments (Figure 3).
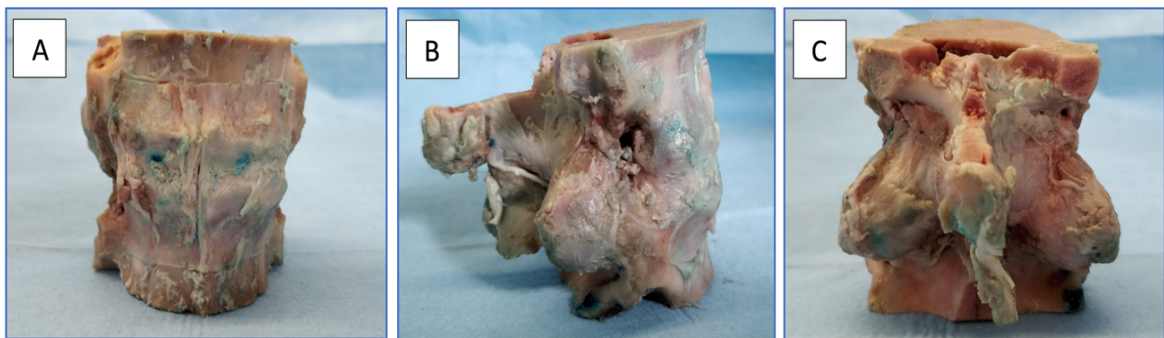

Figure 3. L3-L4 spine segment after soft tissue cleaning. A: Anterior view; B: Lateral view; C: Posterior view.

The segment extremities were potted in 62 x 62 mm acrylic cement powder in order to grip the specimen without damaging it (Figure 4). The cementation was produced with a mix of 40 g PMMA powder and 20 g of monomer. The alignment between intervertebral discs and the PMMA cement had to be parallel and centered with the horizontal plane (Figure 5).
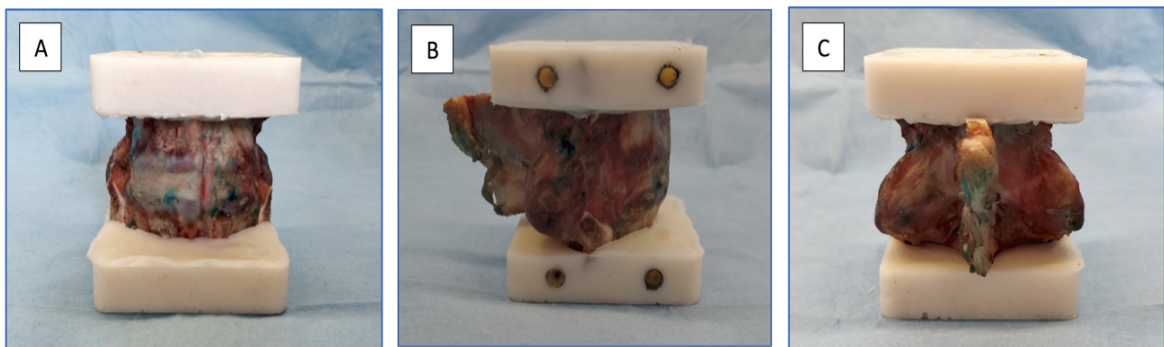

Figure 4. L3-L4 spine segment after PMMA cementation in both extremities. A: Anterior view; B: Right view; C: Posterior view.

In order to use the DIC system appropriately, a high-contrast white-on-dark pattern was dyed in the specimen: a dark preparation of 4 g of methylene-blue mixed with 100 g of water was used to strain the specimen and a white speckle pattern was sprayed using an airbrush-gun on top of the dark background [35].

---

* It has been proved that the number of vertebra in pigs can vary proportionally to their body weight [36]. T13-L1 and T15-L1 are the same 2-level segment but formed with different thoracic vertebrae.
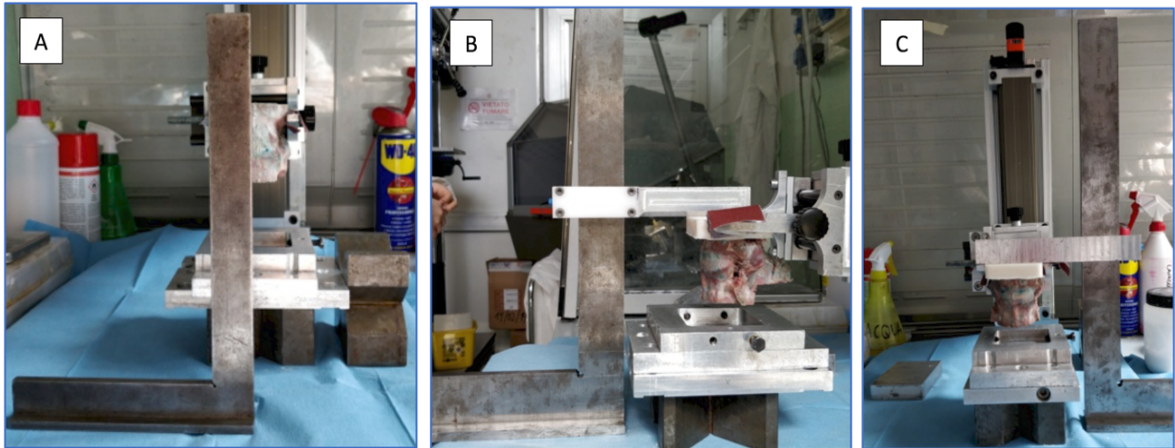
Figure 5. Alignment of an L3-L4 spine segment for the cementation. A: Alignment in height; B: Alignment in depth; C: Alignment in length.

The DIC system is a very sensitive process which requires an optimization of all the parameters and characteristics of the specimen. Due to that, the preparation of the airbrush-gun has already been studied and settled on by Palanca et al. optimizing the pattern for the contrast of the specimen [30]:

- 1,2 atm of pressure applied to the gun.
- Paint preparation: 30 % water and 70 % white paint.
- White-on-dark ratio close to 50-50.
- The size of the paint dots had to be 2-3 times the DIC pixel dimension.

This painting method allowed to obtain an efficient correlation in order to test the motion of the spine (Figure 6).
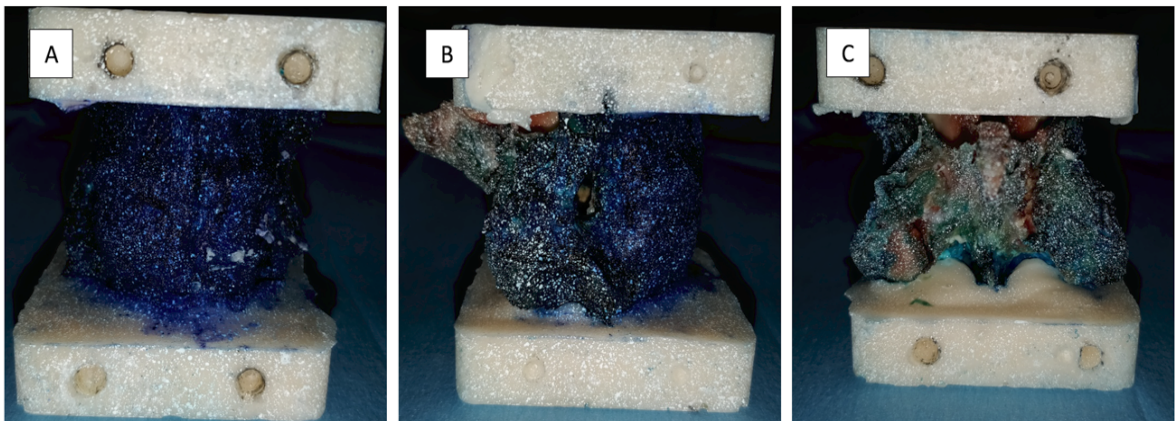

Figure 6. Result of the painting and alignment of an L3-L4 spine segment. A: anterior view; B: right view; C: posterior view.

Once specimens were prepared, they were kept in a freezer in order to preserve their functional, structural and biological properties.

2.2. Test setup

Once the segment was prepared, it was put on a servo-hydraulic universal loading machine (8032, Instron, High Wycombe, UK) where it was fixed in frontal or lateral view.

The specimen surface was studied with a 3D-DIC system consisting in 2 cameras of 5 MP resolution (Q-400, Dantec Dynamics, Skovlunde, Denmark), equipped with 35 mm lenses (Xenoplan, Schneider-Kreuz-nach, Bad Kreuznach, Germany). The cameras were focused on the same area, each one having an angle of 13º to the floor during the test (Figure 7) and the specimen was brightened with 2 LED lightbulbs in order to improve the contrast in the resulting DIC images (Figure 8).
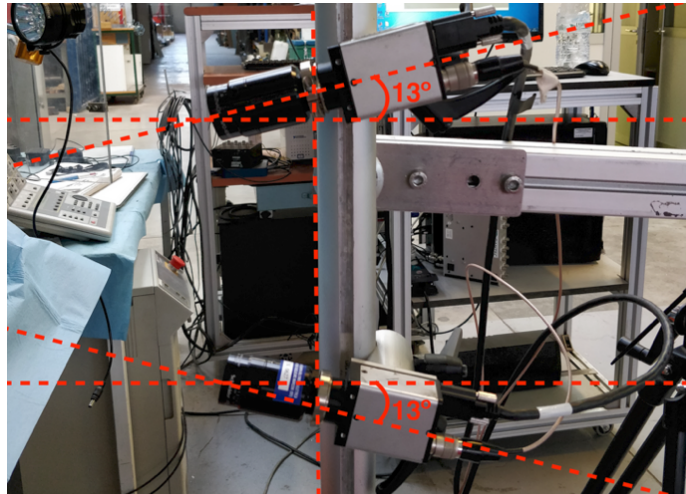
Figure 7. Angle disposition of 3D-DIC cameras.

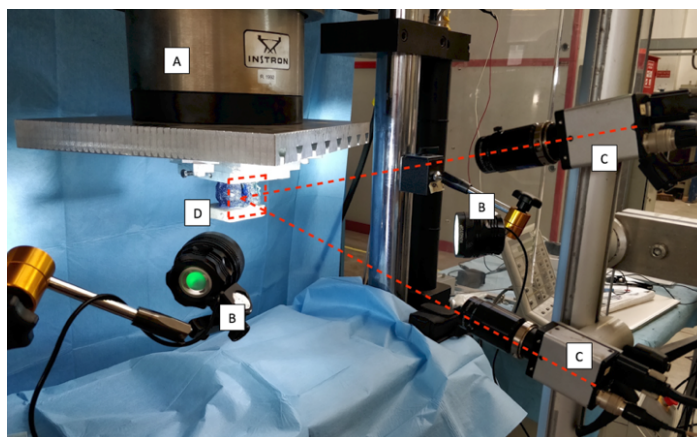*Figure 8. Completed test setup. A: Loading machine; B: LED lightbulbs; C: 3D-DIC cameras; D: ROI of the specimen.*

Both cameras were connected to a computer equipped with Istra-4D software (Dantec Dynamics) specifically designed for DIC applications. This software was used to compute displacements and strains from the recorded images. Before testing, the parameters of DIC computation had to be optimized.

2.3. Error optimization

2.3.1. DIC parameters

From the previously fixed specimen, the DIC cameras are supposed to acquire null changes in the images. However, the digital noise affects the results entailing to an undesired variation in the acquisition.

In order to reduce the noise of the DIC system, two identical photos of the specimen surface under unloaded conditions were taken and the correlation between them performed, adjusting the following parameters (Figure 9):

- The "Facet Size" or the dimension of the computed area: 25, 29, 33 and 35 pixels.
- The "Grid Spacing" or the gap between facets: 7, 11, 15, 19, 22 and 25 pixels.
- The "Local Regression" (regression kernel size) or the extension of the computational domain: 5, 11, 15 and 19 pixels.
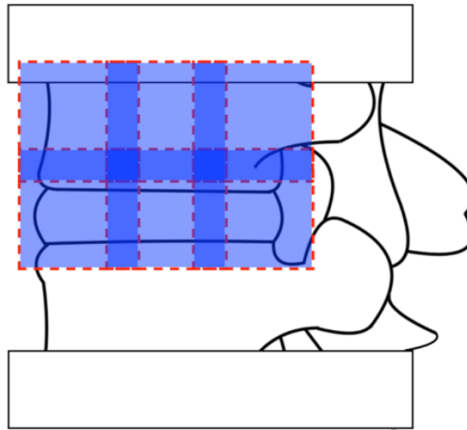

Figure 9. Representation of the parameters for calibration in a lateral view specimen. In low opacity blue it is represented the computed area of the Facet Size and it gets opaquer when the Facet Size is overlapped (Grid Spacing).

In other terms, the Facet corresponds to the subarea of the image with a special pattern where strains will be computed and recognized over time. In order to obtain a continued mapping, the computed areas overlap and this redundancy is defined by the Grid Spacing. Once the strains are computed, a smoothing of the results is performed among the filters proposed by the software. In particular, it is used a local filter with different kernel size called Local Regression.

The parameters values were selected based on previous results from Palanca et al., in particular focusing on the area with the smallest total error: increasing any parameter reduces the error on the computed strain [30]. The values of these parameters gave an extended range of options to find the optimal solution.

2.3.2. DIC optimization outputs

The objective of finding the optimal parameter combination was to reduce the most the noise of the DIC images taken or total error. The ideal result of this test was to obtain the maximum correlation between both cameras, and this entails to have the minimum error in the results.

Using the Istra-4D software it was possible to visualize both cameras acquisition and to perform the correlation in a selected area. For each combination of parameter values, the systematic and random errors of the first and second true principal strains (e1 and e2 respectively) were measured (Figure 10). Once the error values were recorded, the results were plotted in 3D in Matlab (MathWorks) to perform the analysis (read 3.1.).
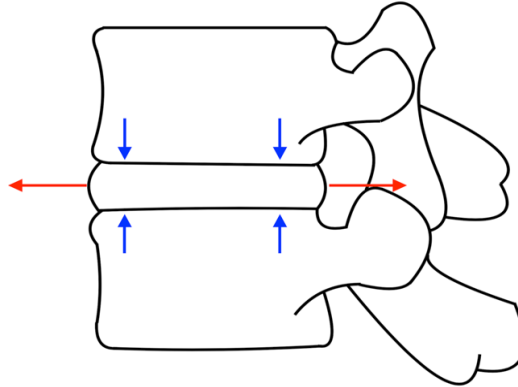

Figure 10. Representation of e1 (blue) and e2 (red) principal strains. For loading conditions (read 2.4.5.2.), they are named transversal (red) and axial (blue) strains.

2.4. Test

Once the DIC software parameters were derived, the loading test was carried out. The optimization had to be identical to the test in order to have the optimized results in the DIC correlation. It was necessary to previously defrost completely the specimens in order to have reliable tests.

2.4.1. Calibration

After the defrosted specimen was fixed in the loading machine and the DIC cameras were installed, a calibration was required in order to define the orientation system in the DIC during the specimen motion. The calibrator consisted of a plate with a black and white pattern and the axes recognized by the DIC software (Figure 11). The calibration was performed using the studied optimal parameters (read 4.1.).
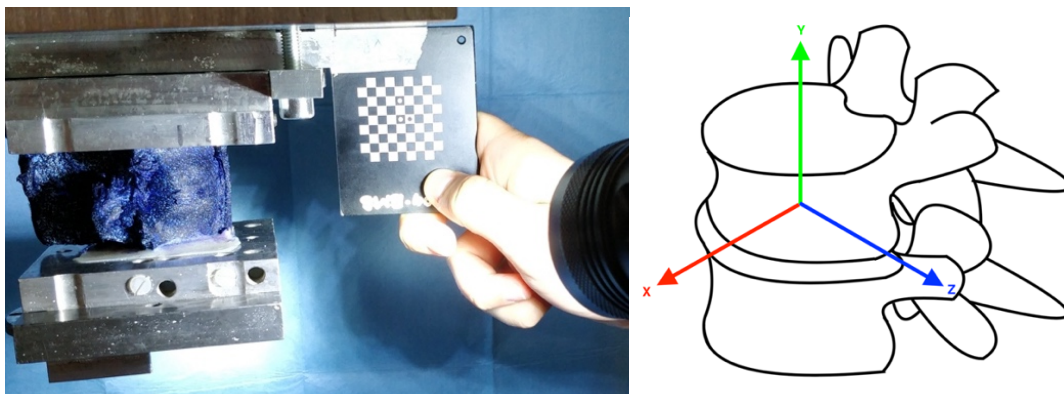

Figure 11. Calibration procedure. It needed to define the space frame (left) and reference system (right). Red: X axis; Green: Y axis; Blue: Z axis.

2.4.2. Motion

After the calibration, the correlation was performed based on 2 pictures before applying any load in order to assure that the specimen was in good conditions to be correlated.

Then, the specimen was put in a pre-conditioning load consisting of 20 cycles of 200 N with a 0.5 Hz frequency to prepare the specimen for the test. The preconditioning is applied to remove any remaining effect of freezing and reach a steady state. Once the pre-conditioning was done, 6 loading cycles of 200 N ($\approx$ 5.4 Nm) were applied in flexion, extension and lateral bending. Each test has been reproduced twice. Loading tests consisted of a ball and socket joint applied in the lower vertebra and the test was repeated twice with the aim of getting reproducibility. In the test, it was ideal that the upper vertebra was fixed (Figure 12).
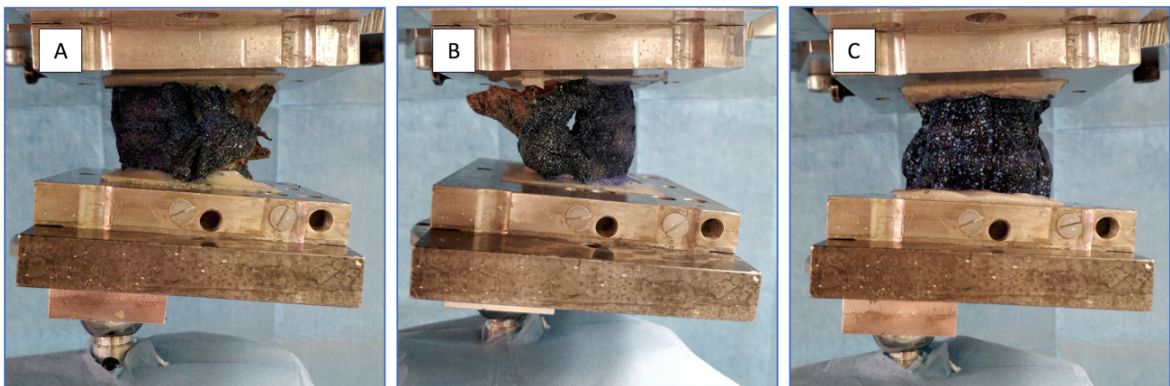

Figure 12. Different loading test dispositions applied to an L3-L4 segment in order to replicate the human motions. A: Flexion; B: extension; C: Lateral bending.

The testing machine was displacement-control driven: the load magnitude was manually reached from an initial load of 2N and the displacement between the 2N and 200N was recorded and applied as the input of the test. However, the approximation of this method can be compromised entailing to a wrong magnitude. This problem was solved with a previous custom Matlab code that extracted the 200 N loading level in order to compute the variables of every test in the same conditions.

While the load was being applied, the Instra-4D was recording pictures at a 15 Hz frequency and through LabVIEW (National Instruments) the load and displacement were recorded at 500 Hz.

2.4.3. Nucleus pulposus extraction

The specimens have been tested in different conditions: healthy, in a degenerated simulated state, and cemented. Simulate a degenerated disc was artificially done by manually extracting the nucleus. The procedure consisted of reaching the nucleus digging into the annulus fibrosus in the opposite side of the region of interest of the specimen using a scalpel (Figure 13). A hole of about 5 x 5 mm was performed and served to remove the nucleus pulposus.

After removing the nucleus pulposus completely, specimens were loaded in the same conditions as the previous tests and were recorded on the intact specimen surface.
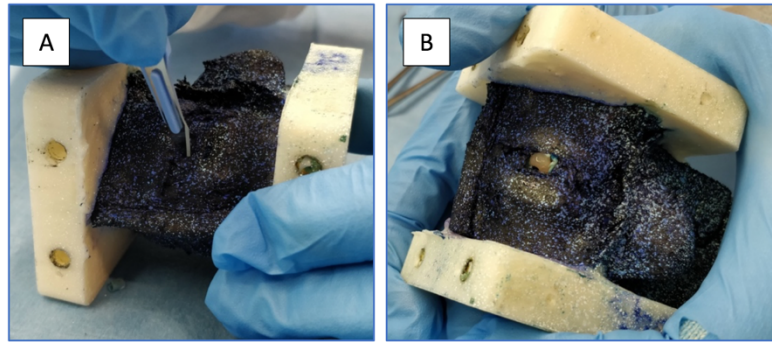
Figure 13. Nucleus pulposus removal procedure. A: With a scalpel, it is made a puncture in the annulus fibrosus in the opposite side of the region of interest of the specimen; B: The nucleus pulposus comes out of the puncture when is applied a compression.

2.4.4.   Cementation

Once the loading test was applied in the unhealthy or degenerated specimens, intervertebral discs were filled with PMMA cement using a syringe (Xtruder, Tecres) while positioned in tension in order to gain height (Figures 14A and 14B). The injection was stopped when the cement leaked from the disc. After the PMMA injection, the specimen was scanned using micro-CT to visualize the position of the cementation inside the intervertebral disc (Figures 14C and 15).
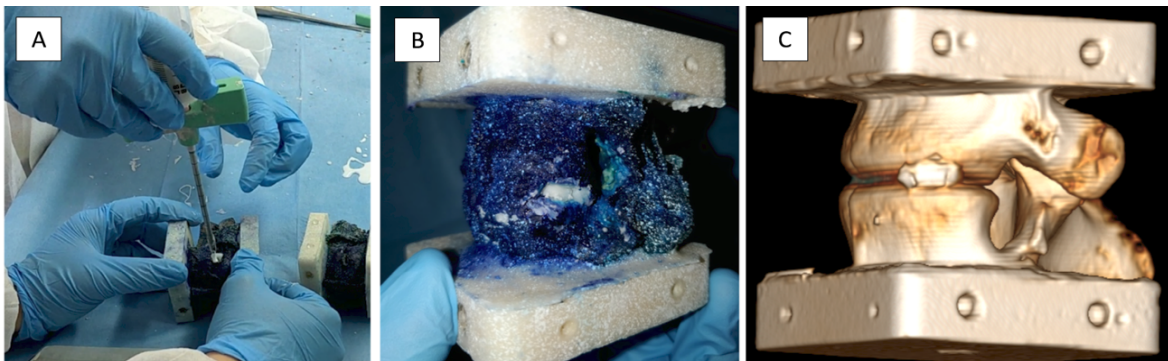
Figure 14. Intervertebral disc cementation procedure. A: Injection of the cement in the puncture while the specimen is manually positioned in tension; B: Result of the cementation; C: Specimen micro-CT reconstruction.
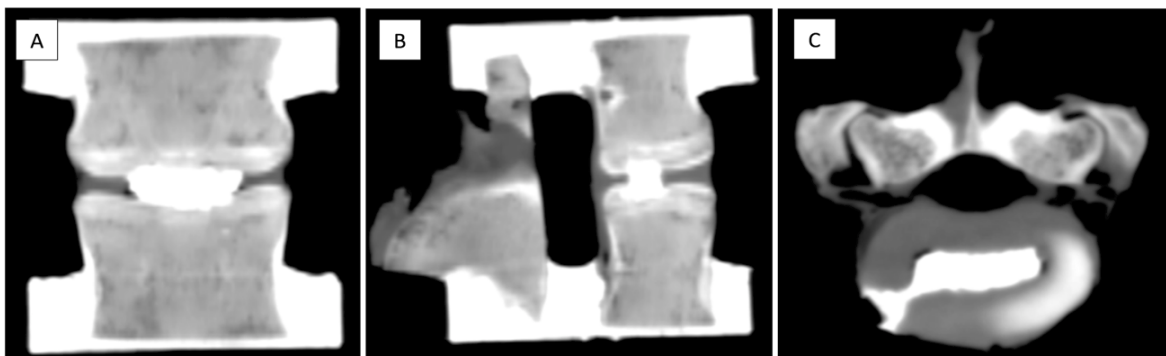
Figure 15. DICOM images from a specimen after cementation. A: Coronal view; B: Sagittal view; C: Axial view.

After the cementation, specimens were loaded in the same conditions as the previous test and were recorded on the intact specimen surface.

2.4.5. Test outputs

There were 198 tests in total (18 tests for each one of the 11 specimens). The DIC pictures were correlated and tested using the Instra-4D software and several custom-written Matlab code that consisted of extracting information about the load-displacement correlations. From the imported and treated data through Excel (Microsoft office), the outputs of interest were:

- Height of the intervertebral disc or distance between both vertebrae at 6th peak load.
- DIC strain: average, maximum and minimum strain values in the intervertebral disc at 6th peak load.
- Relative rotation (ROM) and translation (TR): rotation and movement of the lower vertebra compared with the upper vertebra.
- Viscosity: qualification of the impact of the fluid resistance to deformation.
- Micromotion: error or movement of the upper vertebra.

2.4.5.1. Intervertebral disc height

After the specimens were correlated, 2 methods were applied to measure the intervertebral disc height:

- Profile method: consisted of extracting the z-coordinate values from a manually drawn line perpendicular to the intervertebral disc in the specimen DIC surface (Figure 17B) and manually selecting the intervertebral disc bounds through the "ginput" Matlab code that calculates the distance between both selected points (Figure 16). Since this method requires operator intervention, the intra and inter-operator influence has been tested.
- Strain method: consisted of identifying directly the disc limits on the 3D model of the segment reconstructed by the Instra-4D (Figure 17C).

Both methods were applied at the 6th peak load condition, in the last maximum motion, by 2 operators. Outliers were removed according to Peirce's criterion based on probability theory [37]. Due to the nature of the results obtained by two related methods and operators, their reliability was tested applying the Wilcoxon Rank-Sum Test Matlab code "signrank" useful for obtaining the p-value of paired sample procedures [38]. The disc heights in degenerated and cemented conditions have been normalized by the corresponding healthy disc height.
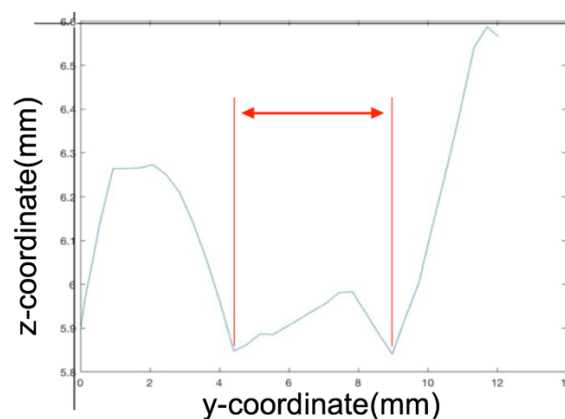

Figure 16. Matlab representation of the profile height method. The x axis represents the drawn line length in mm (y axis in the reference system); the y axis represents the depth of the profile in mm (z-coordinate values). Using the ginput Matlab function, 2 points were located in the intervertebral disc extremes and then it was calculated the distance between them (red).

2.4.5.2.   DIC strain

The true principal strains (transversal and axial) at the surface of the intervertebral disc surface were measured by drawing an area corresponding to the intervertebral disc on the 3D DIC correlation at the 6th peak load for each test (Figure 17). Once selected the area, the Instra-4D software gave the mean, maximum and minimum strain values over the delimited region.

The strain outliers were removed again according to Peirce's criterion based on probability theory [37].
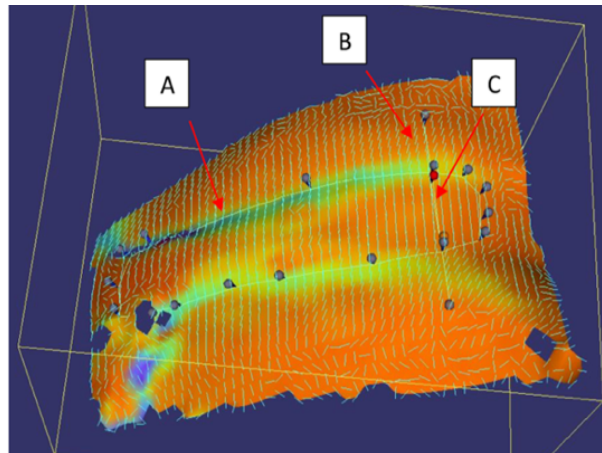

Figure 17. DIC strain representation in a specimen surface. A: Intervertebral disc profile; B: Profile height method; C: Strain height method.

2.4.5.3.   Relative rotation and translation, viscosity and micromotion

From the correlated DIC map of strains, the operator easily identifies both vertebras using a custom-written Matlab code (Figure 18). Assuming the vertebra as rigid bodies, the motion of the lower vertebra mass center is tracked and allows to identify the unloaded and loaded peaks. With this information, it was possible to interpret the data obtaining the following outputs:

- Relative rotation and translation: normalized movement (% of intact) of the lower vertebra in 6 axes, in particular, the relative rotation in the z-axis (ROM) and the relative translation (TR) or vertical movement along the y-axis produced. Outliers were also removed according to Peirce's criterion and after that its reliability was tested applying the Wilcoxon Rank-Sum Test Matlab previously mentioned.
- Viscosity: difference between valley y-coordinate values. If the value changes it means that the viscosity has an impact during the test. Outliers were also removed according to Peirce's criterion.
- Micromotion: unexpected movement of the upper vertebra during the motion respect to the setup. It was calculated measuring the movements of the selected upper vertebra area, the setup being assumed fixed in the ground frame. Outliers were also removed according to Peirce's criterion.
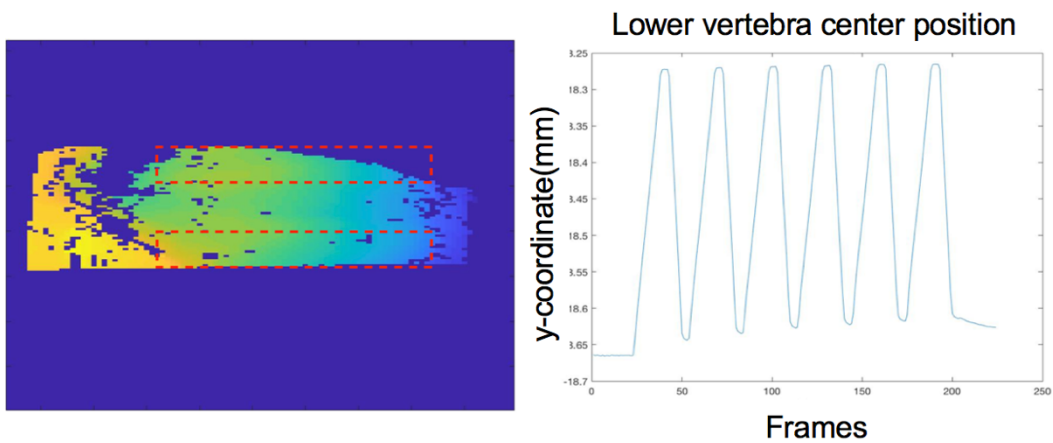
Figure 18. Selection of the upper and lower vertebrae on Matlab (left) and computed lower vertebra motion (right). The ROI of the specimen was the right view, where it is represented the facet joint in yellow and the anterior longitudinal ligament in the opposite side in blue. Loading peaks corresponded to the upward movement of the lower vertebra. For the upper and lower vertebrae mask criterion it was important to select just the vertebra avoiding other components.

3. RESULTS

3.1. Finding the optimal parameter combination

3.1.1. Total error for e1 strain

The first parameter to be fixed was the Facet Size. For all the tested values, the e1 strain decreases inversely with the Local Regression kernel size (Figure 19). Moreover, varying the Grid Spacing from 7 to 22 Grid Spacing pixels, the e1 strain has a U-shape with a minimal value between 7 and 15 Grid Spacing values. On the contrary, for the highest Facet Size, the maximum strain is recorded with the smallest Grid Spacing.

Finally, the minimum values for 25, 29, 33 and 35 Facet Size pixels were 200, 150, 150 and 125 microstrains (μstrain) respectively.

3.1.2. Total error for e2 strain

The total error of the true e2 strain has also been recorded for all the combinations of Facet Size, Grid Spacing and Local Regression (Figure 20). Similar trends as for e2 strain were observed. Generally, an increase of the kernel size corresponded to a reduction of the total error. The influence of the Grid Spacing value was less clear. However, the U-shape observed for the e2 strain remained, with the lowest error found for a Grid Spacing between 9 and 22 pixels.

Finally, the minimum values for 25, 29, 33 and 35 Facet Size pixels were 175, 150, 120 and 125 μstrain respectively.

3.1.3. Random and systematic error for both principal strain

To have a better interpretation of the results, the total error was decomposed into the systematic and the random error (Tables 1 and 2). It is observed that lower error values are predominating in higher Local Regression and Facet Size values and lower Grid Spacing values.
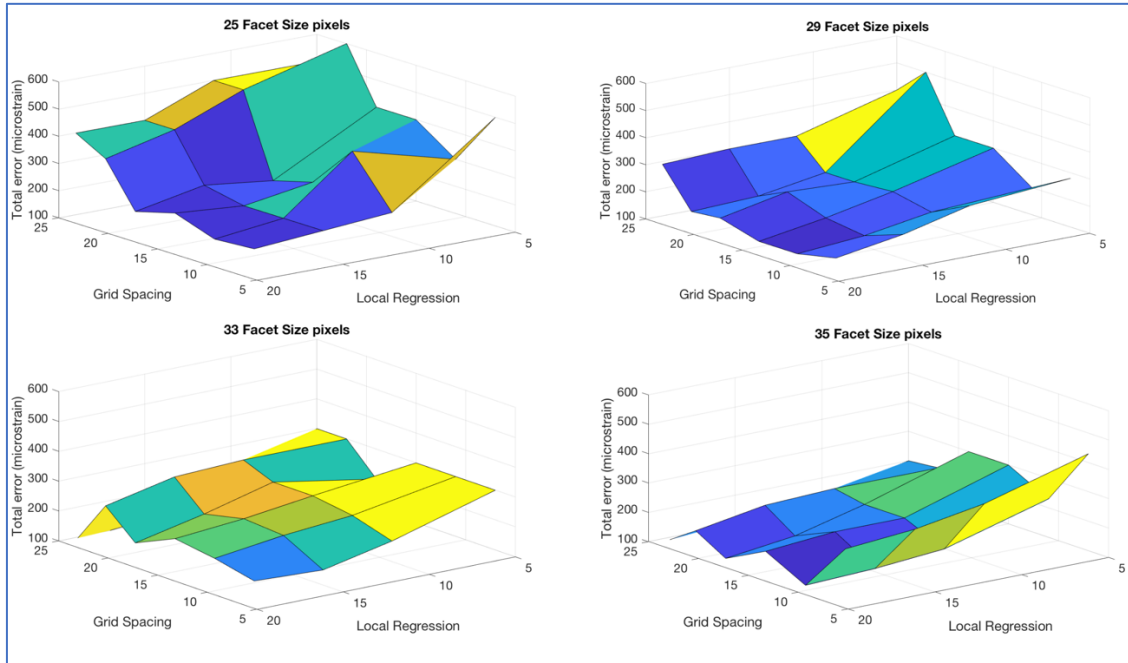

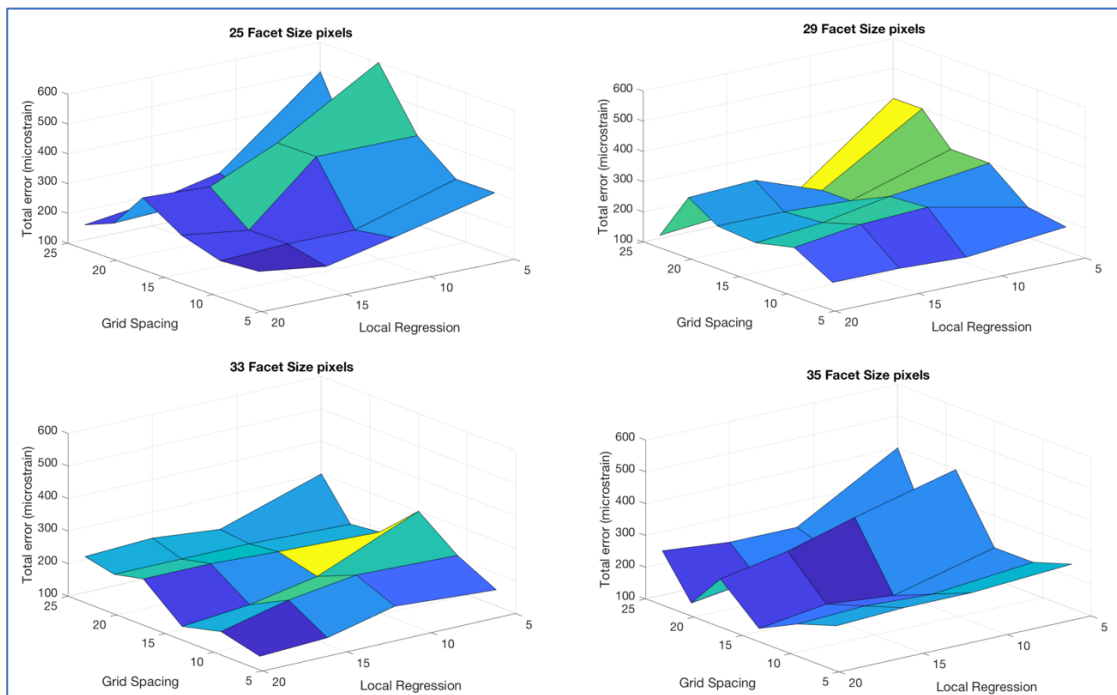*Figure 19. Matlab 3D plots of the total error for the e1 strain.*

Figure 20. Matlab 3D plots of the total error for the e2 strain.

Total error e1 strain		Local regression			
Facet size	Grid spacing	5	11	15	19
	7	200±300	90±130	70±130	60±120
	11	100±200	100±300	0±200	30±140
	15	200±200	70±170	50±150	50±170
	19	0±400	0±200	70±160	50±130
	22	200±400	200±300	200±200	150±190
25	25	0±500	200±300	200±200	200±200
	7	160±120	130+-120	90±100	70±80
	11	40±160	40±140	30±110	30±90
	15	100±200	60±150	40±120	20±100
	19	0±300	0±200	30±180	20±140
	22	100±400	30±170	40±120	40±110
29	25	100±300	100±200	120±180	130±160
	7	140±160	70±130	70±80	70±90
	11	100±200	90±150	90±130	90±100
	15	100±200	80±180	80±150	80±130
	19	0±200	70±190	50±150	30±120
	22	100±200	100±200	120±170	100±140
33	25	0±300	20±130	10±100	0±90
	7	300±130	230±100	200±90	180±90
	11	60±170	40±90	30±80	30±70
	15	100±200	50±140	50±140	50±120
	19	100±200	50±140	30±100	20±80
	22	40±170	50±160	40±160	20±140
35	25	0±200	-10±120	-10±100	0±90

Total error e2 strain		Local regression			
Facet size	Grid spacing	5	11	15	19
	7	100±200	40±180	0±170	-40±160
	11	0±300	0±200	-10±190	-30±160
	15	-100±300	-100±300	0±200	-40±190
	19	-200±400	-100±300	-100±200	-130±180
	22	0±300	0±200	-50±150	-60±130
25	25	-100±400	40±190	40±140	40±110
	7	30±150	-10+±140	-40±120	-50±110
	11	0±200	-100±170	-110±150	-110±120
	15	0±300	-70±190	-60±160	-70±130
	19	0±300	0±200	-30±180	-60±150
	22	-100±300	0±200	-90±190	-100±170
29	25	-100±300	-10±140	-10±120	-10±100
	7	0±150	40±130	20±100	0±110
	11	20±190	70±150	70±120	70±70
	15	-100±200	-10±160	0±130	-10±100
	19	0±190	-10±190	-50±160	-70±140
	22	-20±160	-20±170	-60±130	-80±110
33	25	0±300	0±200	-60±160	-60±150
	7	130±110	150±70	150±70	120±90
	11	-20±180	-50±120	-70±110	-70±100
	15	0±200	10±110	10±130	0±110
	19	-100±300	-130±190	-110±150	-90±130
	22	0±200	10±180	0±140	-10±100
33	25	-100±300	-60±160	-80±140	-110±130

Tables 1 and 2. Total error for e1 (left) and e2 (right) strains separated in systematic and random error respectively.

3.2. Test

3.2.1. Intervertebral disc height

Using the strain method, the normalized degenerated flexion height average (of the 11 specimens) was 88.52 % and 88.95 % for extension. The normalized cemented flexion height average was 93.04 % and 108.19 % for extension (Figure 21 and 22). Small standard deviations values can be disregarded.

Using the profile method, the normalized degenerated flexion height average was 89.39 % and 102.51 % for extension. The normalized cemented flexion height average was 94.82 % and 100.08 % for extension (Figure 22 and 22). Small standard deviations values can be disregarded except for degenerated extension (29 % standard deviation).
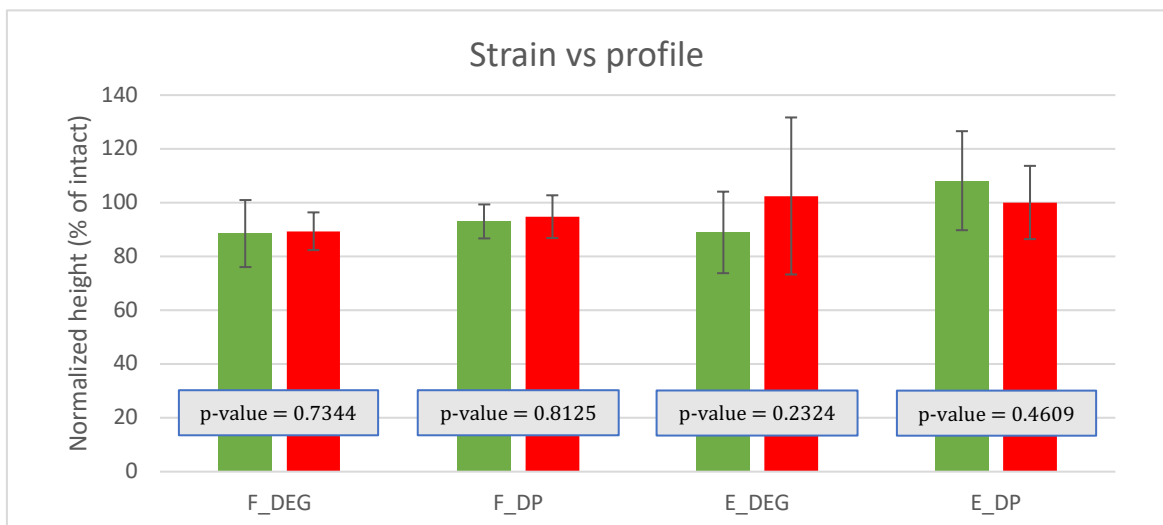

Figure 21. Disc height computed with strain (green) and profile (red) methods.

Comparing both methods, there are no significant differences (Figure 23). Among the obtained results of each method, it was observed significant statistical differences between degenerated and cemented disc in extension for the strain method (Figure 23).
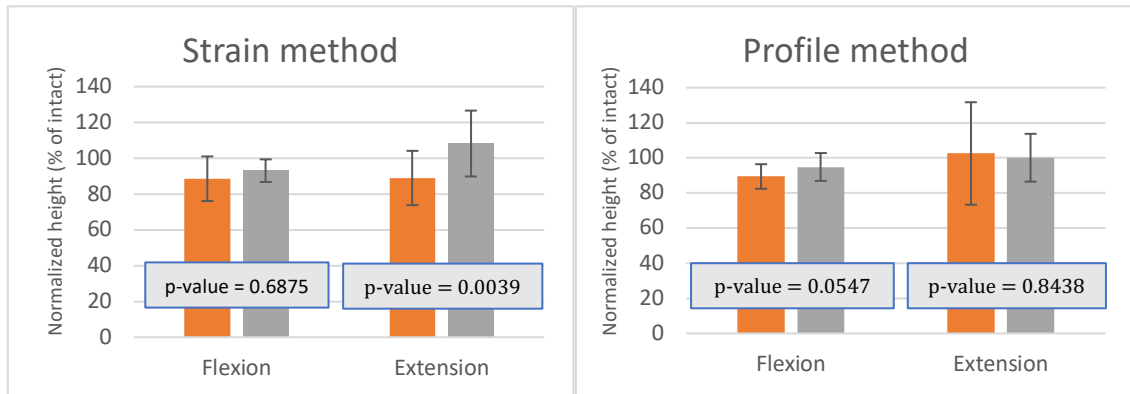

Figure 22. Disc condition comparison with degenerated (orange) and cemented (grey) discs in flexion and extension for strain and profile methods.

Between operators, the operator nº1 obtained 3.99 mm with strain method and 3.73 mm with profile method; the operator nº2 obtained 4.17 mm and 3.78 mm respectively. There were no significant differences between operators for both methods (Figure 22). Small standard deviations values can be disregarded.
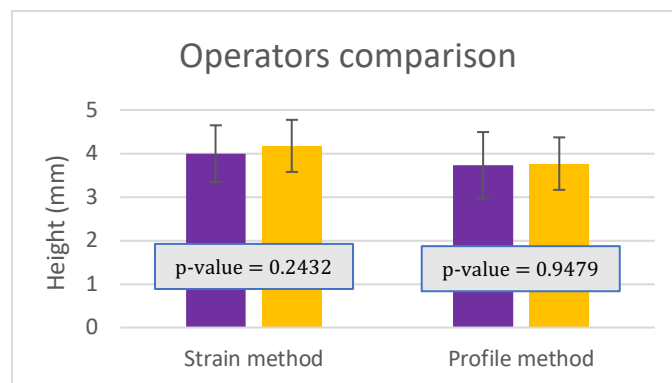

Figure 23. Operators comparison for strain and profile method. Purple: Operator nº1; Yellow: Operator nº2.

3.2.2. DIC strain

Referring to the intervertebral disc strains, the maximum values (intervertebral disc prominence) predominated in transversal strains (Figure 24) and the minimum values (intervertebral disc compression) in axial strains (Figure 25). It was also observed that for both strains average values had no significant differences.
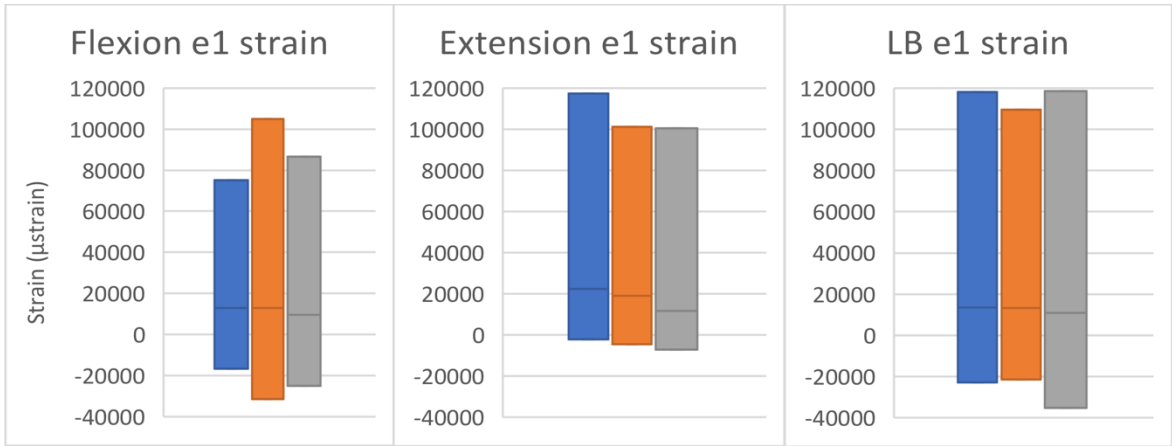
Figure 24. Transversal (e1) strain. Blue: Intact; Orange: Degenerated; Grey: Cemented. The upper side of the box represents the maximum value; the lower side of the box represents the minimum value; and the midline of the box represents the mean.
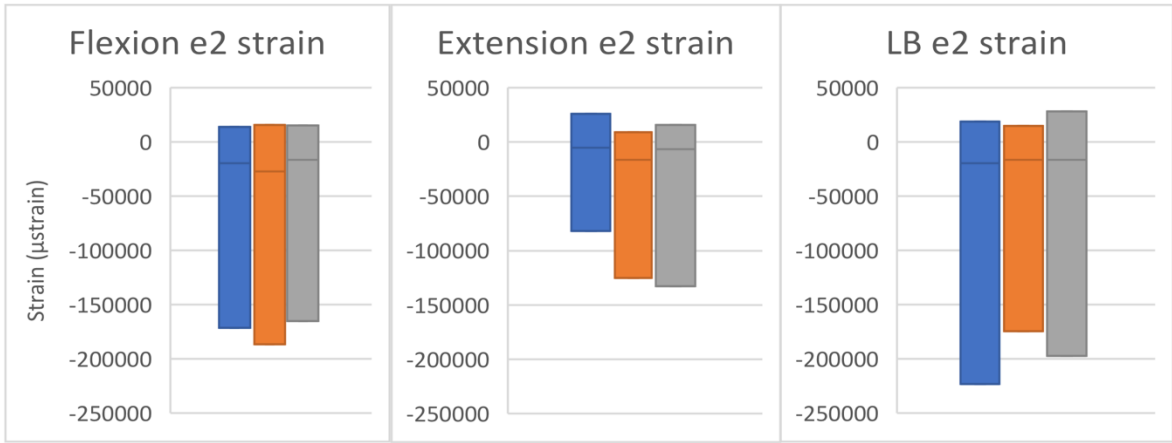
Figure 25. Axial (e2) strain. Blue: Intact; Orange: Degenerated; Grey: Cemented. The upper side of the box represents the maximum value; the lower side of the box represents the minimum value; and the midline of the box represents the mean.

3.2.3. Relative rotation and translation

The intact ROM in flexion, extension and lateral bending were about 2.13º, 2.71º and 1.84º respectively with 0.98, 1.46 and 1.5 standard deviation respectively (Figure 26).
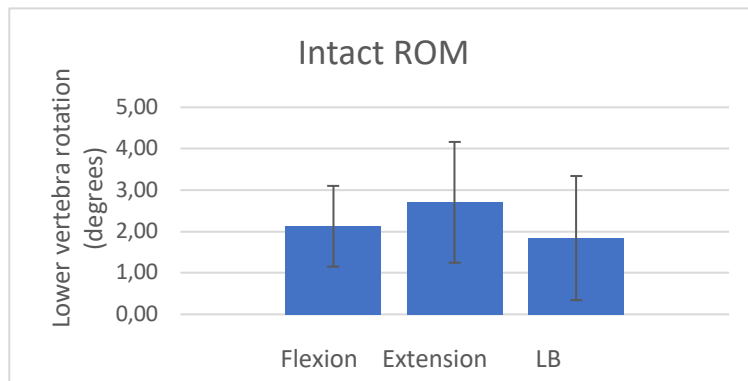

Figure 26. ROM of intact specimens in degrees for flexion, extension and lateral bending.

For the normalized ROM comparing with intact values (Figure 27), degenerated specimens presented 86.32 % (25.71 standard deviation), 110.77 % (26.05 standard deviation) and 90.58 % (27.34 standard deviation) of the intact ROM in flexion, extension, and lateral bending respectively. On the other hand, cemented specimens obtained 80.16 % (14.46 standard deviation), 108.28 % (43.23 standard deviation) and 104.09 % (29.52 standard deviation) in flexion, extension and lateral bending respectively. There were no significant differences between degenerated and cemented ROM.
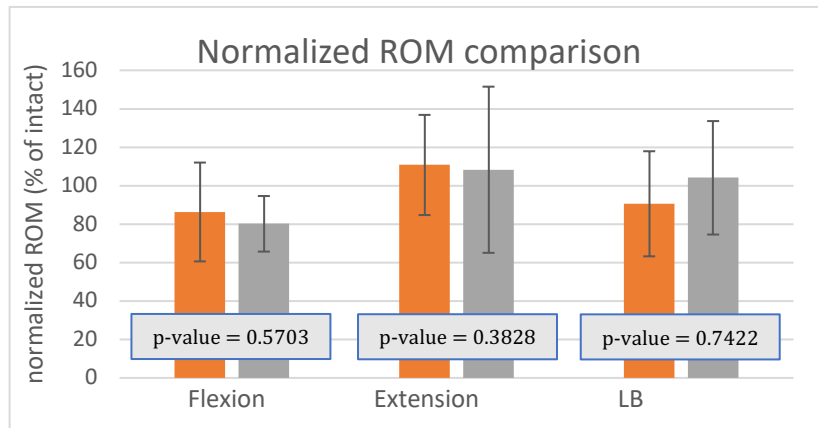

Figure 27. Degenerated (orange) and cemented (grey) normalized ROM comparison for flexion, extension and lateral bending.

The intact TR for flexion, extension and lateral bending reached 0.28 mm, 0.94 mm and 0.41 mm respectively with 0.28, 0.74 and 0.4 standard deviation respectively, being higher in extension (Figure 28).
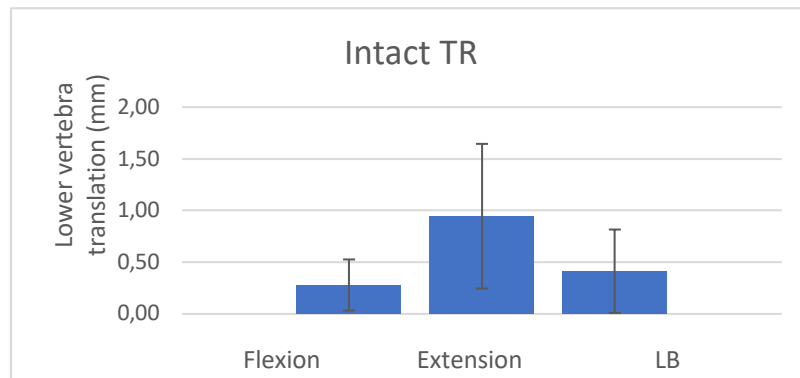
Figure 28. TR of intact specimens in mm for flexion, extension and lateral bending.

For the normalized TR comparing with intact values (Figure 29), degenerated specimens obtained 109.8 % (83.82 standard deviation), 123.38 % (145.35 standard deviation) and 100.79 % (58.15 standard deviation) in flexion, extension and lateral bending respectively. On the other hand, cemented specimens obtained 165.64 % (180.2 standard deviation), 143.62 % (138.5 standard deviation) and 86.49 % (73.01 standard deviation) in flexion, extension and lateral bending respectively. It was observed that the results were so irregular with high standard deviation values.
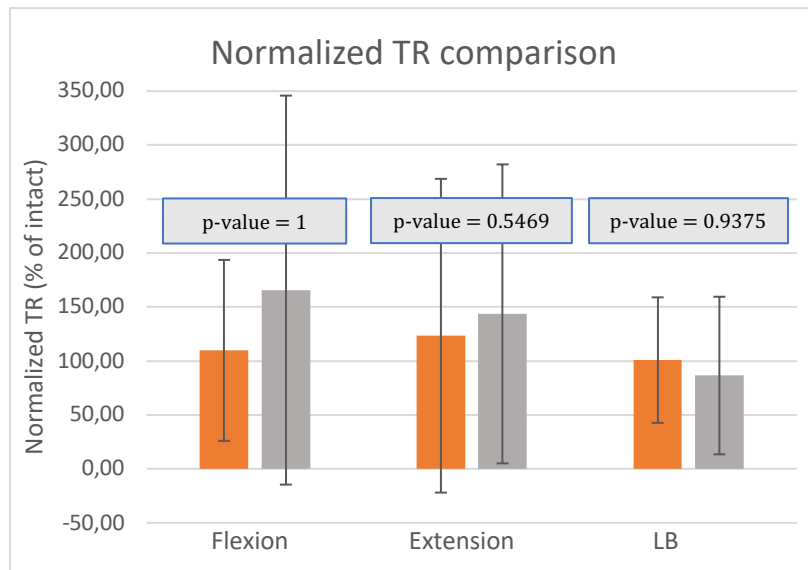
Figure 29. Degenerated (orange) and cemented (grey) normalized TR comparison for flexion, extension and lateral bending.

3.2.4. Viscosity and micromotion

Viscosity and micromotion results were represented simultaneously given their definition of variables with almost negligible values (Figures 30 to 33).

Figure 30. Viscosity ROM comparison for flexion, extension and lateral bending in every axis. Blue: Intact; Orange: Degenerated; Grey: Cemented.

Figure 31. Micromotion ROM comparison for flexion, extension and lateral bending in every axis. Blue: Intact; Orange: Degenerated; Grey: Cemented.

22

Figure 32. Viscosity TR comparison for flexion, extension and lateral bending in every axis. Blue: Intact; Orange: Degenerated; Grey: Cemented.
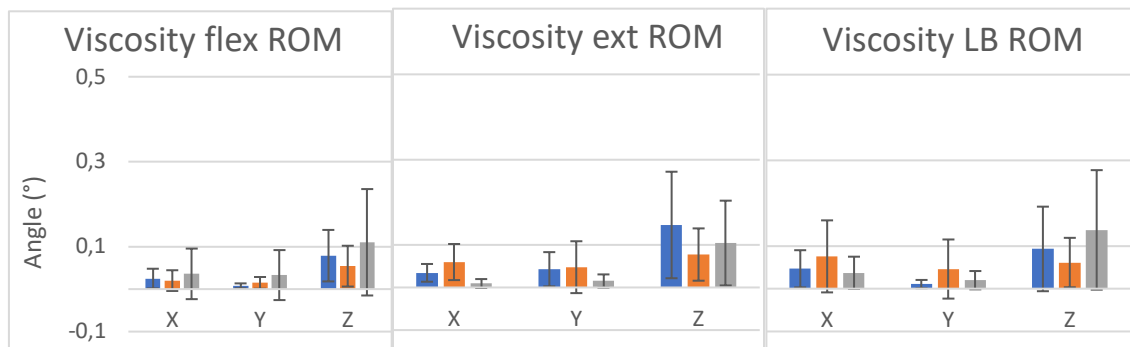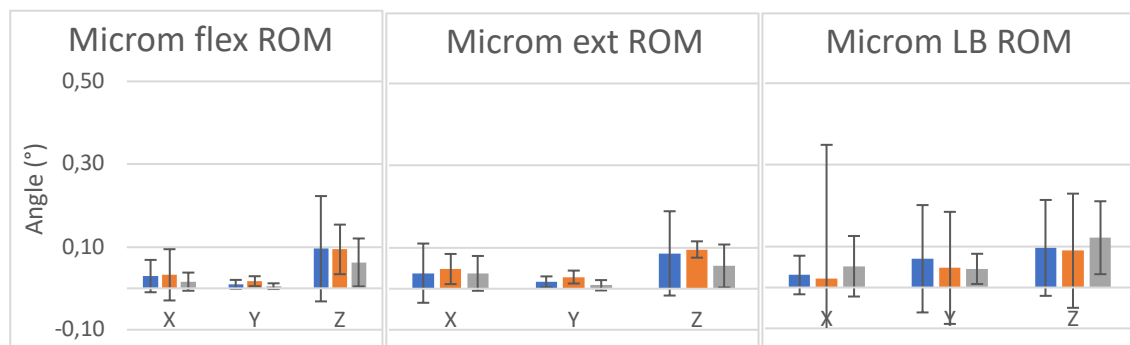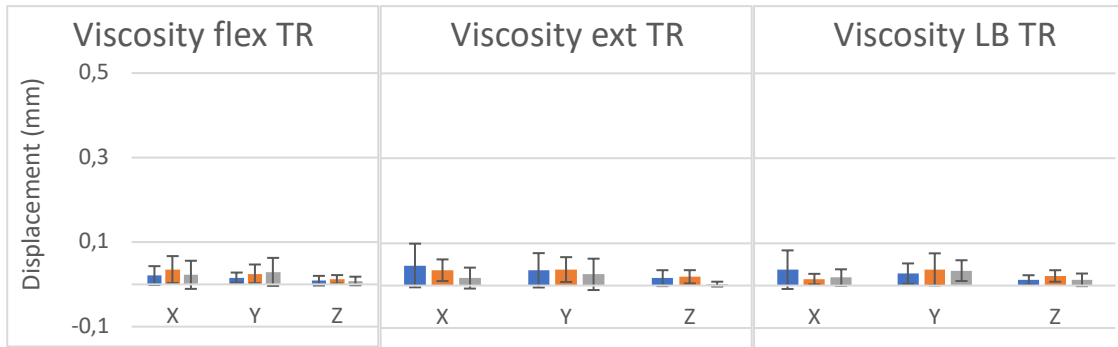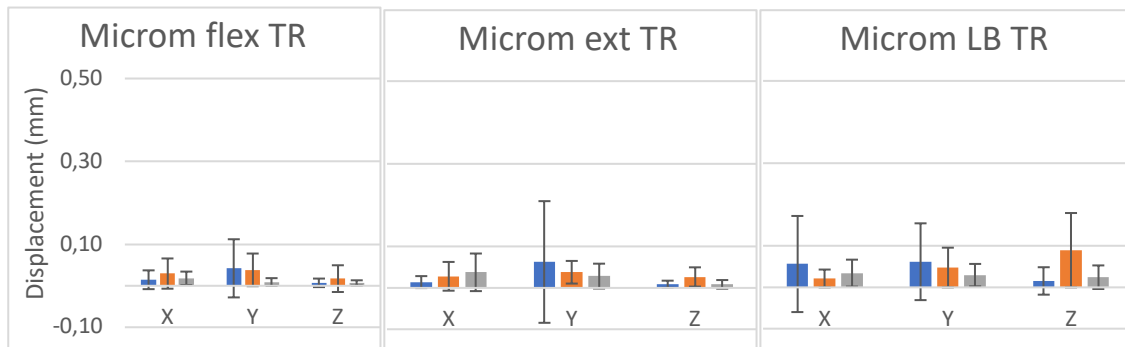

Figure 33. Micromotion TR comparison for flexion, extension and lateral bending in every axis. Blue: Intact; Orange: Degenerated; Grey: Cemented.

4. DISCUSSION

4.1. Optimal parameters

Both principal strains (Figures 19 and 20) showed minimized random and systematic errors when the Local Regression was higher. This is because high Local Regression values entail to higher filtering, smoothing the computerized area and reducing the error. However, the interesting strain values can be harmed by aggressive filtering.

Furthermore, the systematic error experienced lower values with higher Facet Size when the Grid Spacing is maximum. On the other hand, the random error is decreased with higher Facet Size values but increased with higher Grid Spacing values (Tables 1 and 2).

As it has been said earlier, this study overlaps with the parameters used by Palanca et al. [30]. The results of this study confirmed the values previously found, with similar trends for axial and transverse strains. However, the trends were less regular than previously. This can be explained by the larger range of investigated parameters which reveals the successive decrease and increase of the error when increasing the Grid Spacing. Moreover, those variations remained below 250 µstrains (lower than Palanca et al. results), this could be because of the higher resolution compared with Palanca et al. values, and that entails to a small noisy fluctuation that can be despised.

23

To optimize the DIC process, the total error was reduced. However, among the lowest total error combinations, the optimized coupling parameters were selected by compromising the random and systematic error values. Both of them had to be small even if they did not show the smallest values within the pre-selected values. According to this and considering the Local Regression issue, the best combination of parameters to apply in the loading test was:

- Facet Size: 35 pixels.
- Grid Spacing: 11 pixels.
- Local Regression: 5 pixels.

4.2. Test

4.2.1. Intervertebral disc height

Comparing the strain and profile methods, the values for each motion are more or less similar except for extension, where there are some differences but no significant. Comparing subjectively, the strain method was thought to be more reliable to measure the height because it was easier to the operators to distinguish the correlated intervertebral disc surface (Figure 17) compared with the profile method (Figure 16). Between operators, differences were not significant in both methods.

Observing the strain method results, it is highlighted that the PCD recover the loss of height due to the degeneration, providing a 4.52 % of the increase in flexion and 19.34 % in extension from the degeneration to the discoplasty. Only the recovery in extension was significant. This confirms that PCD has the purpose it was initially used for.

4.2.2. DIC strain

For transversal and axial strains (Figures 24 and 25), it has to be considered that soft tissue has a high risk of failure when it is applied to a load. In degenerated specimens in flexion strain values are higher and that can lead to tearing the disc, but intact values are recovered with discoplasty. However, there are some exceptions as the axial strain for extension and the transversal strain for lateral bending where discoplasty compress more the tissue than in the other conditions. Regarding the average strain values, it was observed insignificant differences.

It has to be considered that axial strain is defined by the tensile or compressive displacement and the transversal strain is defined by the bulge or hollow generated in the disc during the motion (Figure 9). This could explain that absolute axial strain values are higher than absolute transversal strain values because of the motion that is applied.

4.2.3. Relative rotation and translation

Regarding the intact ROM values (Figure 26), the obtained flexion and extension ROM were approximately the observed by Lysack et al. in a multi-segmental pig lumbar model, where applying 5 Nm it is obtained 2.5º in both motions [39].

For normalized ROM values (Figure 27), it is not observed significant differences between degenerated and cemented. However, it is observed a mobility improvement with PCD in extension and lateral bending. Discoplasty does not seem to impact the ROM.

On the other hand, the relative translation seems to be so irregular with high p-values, high standard deviation (that could not be corrected with Piece's criterion) and not following a regular trend (Figure 29). An explanation could be imperfections that may have occurred during the specimen preparation procedures as an incomplete extraction of the nucleus pulposus or an incomplete cementation filling that can lead to an irregular compression behaviour. The low number of test repetitions could be a factor as well (read 4.2.5.).

Comparing the relative translation results with the relative rotation, it is observed that when the ROM is blocked by the cement, the rotation is transformed in an axial translation, having an inverse trend as a result.

4.2.4.   Viscosity and micromotion

As we said in the previous viscosity and micromotion results (Figures 30 to 33), their values are negligible compared with the relative rotation and translation. Therefore, it can be assumed that the viscosity of the specimen does not influence the computations of the ROM.

Regarding to the micromotion values, it can be assumed that the upper vertebra is fixed, and it is not involved in the motion.

4.2.5.   Limitations

Among the experiment conditions, it has to be considered that the environment illumination could affect the acquisition of the DIC cameras due to the climatic variance during the project. It would be recommended to isolate the setup from external lightning.

Although animal models have been validated as an alternative to human models [9], [19], experimental observations may differ between porcine and human models. It would be recommended to apply the applied methodology in this study in human models to obtain reliable clinical results.

It is important to remark that every motion was repeated twice to achieve reproducibility as we said previously (read 2.4.2.). However, it is recommendable to reiterate each test 3 times or more because of the difficulty of determining which of the 2 same tests with significant differences has atypical values. Due to the limited time of internship, the study was carried out repeating twice and that could explain the huge dispersion in some experimental data.

Finally, it has to be considered that the removal of the nucleus pulposus and the cementation were manually performed. This procedure is not entirely effective, so it is required to find better alternatives to proceed with both methods.

5.   CONCLUSION

In this study, an optimization of the DIC method has been performed as an alternative to other techniques as FEM or intradiscal transducer and obtaining as result a precise non-invasive method that demonstrates its capacity to be applied in a wide range of biomechanical experimentations.

Regarding the model used in the project, the easiness of obtention of pig models could increase the number of investigations and developments of new surgical methods. However, further human experimentation is needed to become a reliable surgical application.

In conclusion, this study has proved that PCD for degenerated intervertebral discs improves the recovery of height without significant differences in terms of ROM. This intervertebral disc height increase is especially observed in extension, where the vertebral foramen size is less closed than in degeneration, so this could entail to a decreased spinal nerve damage, in other words, PCD could reduce the LBP.

6.   REFERENCES

[1]   J. A. Waxenbaum and B. Futterman, "Anatomy, Back, Lumbar Vertebrae," in StatPearls, Treasure Island (FL): StatPearls Publishing, 2019.

[2]   D. Hoy et al., "A systematic review of the global prevalence of low back pain," Arthritis Rheum., vol. 64, no. 6, pp. 2028–2037, 2012.

[3]   M. A. Adams, "Biomechanics of Back Pain," Acupunct. Med., vol. 22, no. 4, pp. 178–188, Dec. 2002.

[4]   M. A. Adams and P. Dolan, "Spine biomechanics," J. Biomech., vol. 38, no. 10, pp. 1972–1983, Oct. 2005.

[5]   J. A. Buckwalter, "Aging and Degeneration of the Human Intervertebral Disc," Spine, vol. 20, no. 11, p. 1307, Jun. 1995.

[6]   H. J. Christie, S. Kumar, and S. A. Warren, "Postural aberrations in low back pain," Arch. Phys. Med. Rehabil., vol. 76, no. 3, pp. 218–224, Mar. 1995.

[7]   P. N. Sambrook, A. J. MacGregor, and T. D. Spector, "Genetic influences on cervical and lumbar disc degeneration: A magnetic resonance imaging study in twins," Arthritis Rheum., vol. 42, no. 2, pp. 366–372, 1999.

[8]   J. C. Iatridis, S. B. Nicoll, A. J. Michalek, B. A. Walter, and M. S. Gupta, "Role of biomechanics in intervertebral disc degeneration and regenerative therapies: what needs repairing in the disc and what are promising biomaterials for its repair?," Spine J., vol. 13, no. 3, pp. 243–262, Mar. 2013.

[9]   P.-P. A. Vergroesen et al., "Mechanics and biology in intervertebral disc degeneration: a vicious circle," Osteoarthritis Cartilage, vol. 23, no. 7, pp. 1057–1070, Jul. 2015.

[10]   M. Adams and P. Roughley, "What is Intervertebral Disc Degeneration, and What Causes It?," Spine, vol. 31, no. 18, pp. 2151–2161, Aug. 2006.

[11]   M. Adams, D. McMillan, T. Green, and P. Dolan, "Sustained Loading Generates Stress Concentrations in Lumbar Intervertebral Discs," Spine, vol. 21, no. 4, pp. 434–438, Feb. 1996.

[12] R. Gunzburg et al., "A cadaveric study comparing discography, magnetic resonance imaging, histology, and mechanical behaviour of the human lumbar disc," Spine, vol. 17, no. 4, pp. 417–426, Apr. 1992.

[13] P. Pollintine, P. Dolan, J. Tobias, and M. Adams, "Intervertebral Disc Degeneration Can Lead to 'Stress-Shielding' of the Anterior Vertebral Body," Spine, vol. 29, no. 7, pp. 774–782, Apr. 2004.

[14] A. Nachemson, "The Effect of Forward Leaning on Lumbar Intradiscal Pressure," Acta Orthop. Scand., vol. 35, no. 1–4, pp. 314–328, Jan. 1965.

[15] H. Wilke, P. Neef, M. Caimi, T. Hoogland, and L. E. Claes, "New In Vivo Measurements of Pressures in the Intervertebral Disc in Daily Life," Spine, vol. 24, pp. 755–62, May 1999.

[16] M. Al-Rawahi, J. Luo, P. Pollintine, P. Dolan, and M. A. Adams, "Mechanical Function of Vertebral Body Osteophytes, as Revealed by Experiments on Cadaveric Spines:," Spine, vol. 36, no. 10, pp. 770–777, May 2011.

[17] B. W. Cunningham, Y. Kotani, P. S. McNulty, A. Cappuccino, and P. C. McAfee, "The effect of spinal destabilization and instrumentation on lumbar intradiscal pressure: an in vitro biomechanical analysis," Spine, vol. 22, no. 22, pp. 2655–2663, Nov. 1997.

[18] M. Palanca, G. Tozzi, and L. Cristofolini, "The use of digital image correlation in the biomechanical area: a review," Int. Biomech., vol. 3, no. 1, pp. 1–21, Jan. 2016.

[19] M. A. Adams, "Mechanical testing of the spine. An appraisal of methodology, results, and conclusions," Spine, vol. 20, no. 19, pp. 2151–2156, Oct. 1995.

[20] M. de Kleuver, F. Oner, and W. Jacobs, "Total disc replacement for chronic low back pain: background and a systematic review of the literature," Eur. Spine J., vol. 12, no. 2, pp. 108–116, Apr. 2003.

[21] R. D. Guyer and D. D. D. M. Ohnmeiss, "Intervertebral Disc Prostheses," Spine, vol. 28, no. 15S, pp. 15–23, Aug. 2003.

[22] R. Kandel, S. Roberts, and J. P. G. Urban, "Tissue engineering and the intervertebral disc: the challenges," Eur. Spine J., vol. 17, no. Suppl 4, pp. 480–491, Dec. 2008.

[23] R. Zhao, W. Liu, T. Xia, and L. Yang, "Disordered Mechanical Stress and Tissue Engineering Therapies in Intervertebral Disc Degeneration," Polymers, vol. 11, no. 7, p. 1151, Jul. 2019.

[24] P. P. Varga, G. Jakab, I. B. Bors, A. Lazary, and Z. Szövérfi, "Experiences with PMMA cement as a stand-alone intervertebral spacer," Orthop., vol. 44, no. 1, pp. 1–8, Nov. 2015.

[25] C. Sola et al., "Percutaneous cement discoplasty for the treatment of advanced degenerative disk disease in elderly patients," Eur. Spine J. Off. Publ. Eur. Spine Soc. Eur. Spinal Deform. Soc. Eur. Sect. Cerv. Spine Res. Soc., Mar. 2018.

[26] A. Rohlmann, T. Zander, H. Schmidt, H.-J. Wilke, and G. Bergmann, "Analysis of the influence of disc degeneration on the mechanical behaviour of a lumbar motion segment using the finite element method," J. Biomech., vol. 39, no. 13, pp. 2484–2490, Jan. 2006.

[27] G. Denozière and D. N. Ku, "Biomechanical comparison between fusion of two vertebrae and implantation of an artificial intervertebral disc," J. Biomech., vol. 39, no. 4, pp. 766–775, Jan. 2006.

[28] S. M. Renner et al., "Novel model to analyze the effect of a large compressive follower pre-load on range of motions in a lumbar spine," J. Biomech., vol. 40, no. 6, pp. 1326–1332, 2007.

[29] J. P. Little, C. J. Adam, J. H. Evans, G. J. Pettet, and M. J. Pearcy, "Nonlinear finite element analysis of anular lesions in the L4/5 intervertebral disc," J. Biomech., vol. 40, no. 12, pp. 2744–2751, Jan. 2007.

[30] M. Palanca, T. M. Brugo, and L. Cristofolini, "Use of digital image correlation to investigate the biomechanics of the vertebra," J. Mech. Med. Biol., vol. 15, no. 02, p. 1540004, Apr. 2015.

[31] T. J. Keating, P. R. Wolf, and F. L. Scarpace, "An improved method of digital image correlation," Am Soc Photogr Rem Sens, vol. 41, p. 10, Aug. 1975.

[32] B. K. Bay, S. A. Yerby, R. F. McLain, and E. Toh, "Measurement of strain distributions within vertebral body sections by texture correlation," Spine, vol. 24, no. 1, pp. 10–17, Jan. 1999.

[33] M. L. Ruspi, M. Palanca, C. Faldini, and L. Cristofolini, "Full-field in vitro investigation of hard and soft tissue strain in the spine by means of Digital Image Correlation," Muscles Ligaments Tendons J., vol. 7, no. 4, pp. 538–545, Apr. 2018.

[34] M. Palanca et al., "Digital volume correlation can be used to estimate local strains in natural and augmented vertebrae: An organ-level study," J. Biomech., vol. 49, no. 16, pp. 3882–3890, Dec. 2016.

[35] M. Palanca, M. Marco, M. L. Ruspi, and L. Cristofolini, "Full-field strain distribution in multi-vertebra spine segments: An in vitro application of digital image correlation," Med. Eng. Phys., vol. 52, pp. 76–83, Feb. 2018.

[36] S. Mikawa et al., "Identification of a second gene associated with variation in vertebral number in domestic pigs," BMC Genet., vol. 12, no. 1, p. 5, Jan. 2011.

[37] S. Ross, "Peirce's criterion for the elimination of suspect experimental data," J Eng Technol, vol. 20, Sep. 2003.

[38] J. D. Gibbons and S. Chakraborti, "Nonparametric Statistical Inference," in International Encyclopedia of Statistical Science, M. Lovric, Ed. Berlin, Heidelberg: Springer Berlin Heidelberg, 2011, pp. 977–979.

[39] J. T. Lysack, J. P. Dickey, G. A. Dumas, and D. Yen, "A continuous pure moment loading apparatus for biomechanical testing of multi-segment spine specimens," J. Biomech., vol. 33, no. 6, pp. 765–770, Jun. 2000.